Jour. Korean Inst. Mining Geol.
V. 19, Spec. Iss., p. 207-226, 1986

Mineralogical Studies on Sulfide Ore Species of the Tong Myeong Tungsten Deposits

Pyeong-Koo Lee,* Chil-Sup So, Se-Hyun Kim,** Seong-Taek Yun** and Moon-Young Kim***

Abstract; The skarn type tungsten deposits in Jechon area are developed in the contact aureole of Jurassic granodiorite and lower Paleozoic limestone beds. The Tong Myeong mine contains scheelite-bearing skarns found at and near the contacts between crystalline limestone and hornfels. Although the skarns are heterogeneous, there are clear patterns in the preferred associations and nonassociations of minerals on all scales. The skarn show a zonal arrangement from limestone to hydrothermal vein as follow: wollastonite skarn, clinopyroxene skarn, clinopyroxene-garnet skarn, garnet skarn, and vesuvianite skarn. Scheelite, abundant in all skarn units except wollastonite skarn and also in quartz veins near orebodies, is everywhere strongly correlated with pyrrhotite. It is implied that it was a stable phase throughout the evolution of the zoned skarns, at least in pyrrhotite-forming environments. Deposition of scheelite was probably widely caused by increasing $a_{Ca^{2+}}$ in the fluid, resulting from associated and interrelated reactions: $FeCl_2$ aq+H_2S aq→FeS+$2H^+$+$2Cl^-$; and $CaCO_3+2H^+ \rightarrow Ca^{+2}+H_2CO_3$.

The spectral reflection powers of nine sulfide species were studied, for three mineralization stage. The shapes and characteristics of the spectral reflectivity profiles are significant in their control of other optical properties. The characteristics of the Vickers microhardness and the optical symmetry for the minerals studied are discussed. Broad radicle groupings of the sulfides can be made with regard to the reflectivity-microhardness values.

INTRODUCTION

The Tong Myeong mine is located in the Songhwak-Myeon, about 10km to the northeast of Jechon, Korea. Many skarn deposits are known in this district. The skarn type tungsten deposits are developed in the contact aureole of Jurassic biotite-hornblende granodiorite and limestone beds. The ore deposits are considered to have been genetically related to granitic magmatism of this pluton.

In recent years, scheelite-bearing skarn deposits have attracted considerable explorationary and academic interest. Newberry and Einaudi(1981) conclude that the commonly high-grade scheelite in hydrous skarns result from the concentration of tungsten originally emplaced in a more dispersed state in prograde skarns. Skarn deposits which are generally characterized by a coarse-grained mixture of calc-silicates formed by metasomatic processes at relatively high temperature, are becoming important as sources of various metals. These calc-silicate rocks often are formed by the replacement of Ca in calcareous rocks by Si, Fe, Mg, and Al. The skarns originated from the hornfels can generally be distinguished from the skarns originated from the crystalline limestone by careful study of field relation, mineral assemblage and its texture, and grain size.

More than 200 polished-thin sections, polished sections, and thin-sections were examined petrographically in transmitted and reflected light

* Korea Institute of Energy and Resources(KIER)
** Department of Geology, Korea University

for the present study. In the present paper, the mode of occurrence and the mineral assemblages of the ore are described. Secondary, reflectivity-microhardness characteristics of the ore studied.

GENERAL GEOLOGY

The geologic setting of the Tong Myeong skarn mining district has been described by Yoshimura, I. (1940), the Geological Investigation Corps of Taebaegsan Region (1962), Kobayashi, T. (1966), and Kim, O.J. (1973), and will not be reviewed in detail here.

The major exoskarn orebody was emplaced in crystalline limestone unit of Ordovician age (Reedman and Um, 1975) following intrusion of late-Jurassic biotite-hornblende granodiorite (Kim, Y.J., 1979). The limestone beds can be divided into the Great Limestone Series of Josen System, Samtaesan Formation and Gabsan Formation which is correlative to the Hongjeom Series of Pyeongan System.

Samtaesan Formation consist mainly of grayish to grayish white limestone and are interbedded with argillaceous, commonly slate and noncalcareous hornfels. The crystalline limestone near skarn zone with no evidence of bedding consists of medium to coarse-grained, a recrystallized limestone unit in which the bulk of the economic scheelite-bearing skarns is developed.

Gabsan Formation was first recognized and named in 1962 by the Investigation Corps of the Taebaegsan Region during their survey. It is composed of shale, sandstone and limestone with impersistent thin beds of conglomerate at or near the base. Samtaesan Formation are overlain disconformably by the base beds of the Gabsan Formation (The Geological Investigation Corps of Taebaegsan Region, 1962; A.J. Reedman, 1975). The metamorphic facies of contact aureole in surrounding rocks adjacent to the granite body are corresponded to hornblende hornfels facies with mineral assemblages of wollastonite-diopside-calcite in calcareous rocks, and of quartz-biotite-muscovite-cordierite in argillaceous rocks (Kim, Y.J., 1979).

Biotite-hornblende granodiorite stocks with generally steeply dipping contacts, and enveloped by extensive thermal contact aureoles, are associated with W-deposits. The intrusions consist mainly of plagioclase ($An_{20\sim40}$), microcline, quartz, biotite and hornblende with minor amounts of sericite, sphene, zircon, chlorite, and scheelite. The exposed portions of the mine stock apparently show local evidence of hydrothermal alteration. K-Ar dates were obtained for muscovite from granodiorite near the mine area. Muscovite from the granodiorite yielded a date of 176 m.y.

SKARNS AND EVOLUTION OF THEIR GROWTH

Outline of skarn formation

Skarn formations are well developed along the contact between the crystalline limestone and hornfels. Skarn formations are largely divided into two original rock types on the basis of subtle variations of relict texture; crystalline limestone and hornfels. The skarns originated from crystalline limestone sometimes include a relict of limestone mass. The limestone is white or gray in color, massive, and recrystallized.

On the basis of mineral assemblages, the skarns originated from crystalline limestone is divided into five units which are zonally distributed. The units from the limestone side to the hydrothermal vein are: (1) wollastonite skarn, (2) clinopyroxene skarn, (3) clinopyroxene-garnet skarn, (4) garnet skarn, and (5) vesuvianite skarn. Scheelit occurs widely in clinopyroxene skarn to vesuvianite skarn except wollastonite skarn. Most scheelite ores are usually contained in the vesuvianite skarn. In general, the zonation patterns of skarns originated from hornfels are ambiguous and irregular.

As well, there is a regularity in the spatial

Table 1 Mineral association of skarns at Tong Myeong desposit.

Skarns	Gangue Minerals		Ore Minerals
	Major	Minor	
Wollastonite	wo	cpx. ga. qtz. cal. chl. mus.	
Clinopyroxene	cpx. amp. qtz.	ga. ves. ep. cal.	sch. po. py.
Clinopyroxene Garnet	cpx. ga.	amp. ves. qtz. cal. chl. ap.	po. py. sp. gn. cpy. mc.
Garnet	ga.	amp. cpx. cal. qtz. ep. chl. ves.	sch. po. py. gn. sp. cpy. bn. witt. bis. bin. mo. cc. cv.
Vesuvianite	ves.	qtz. cal. chl. mus. ga. cpx.	sch. po. py. gn. sp. cpy. bis. bin. gnbi. mc.

Abbreviation: wo=wollastonite, cpx=clinopyroxene, amp=amphibole, ga=garnet, qtz=quartz, ves=vesuvianite, ep=epidote, apt=apatite, cal=calcite, chl=chlorite, mus=muscovite, sch=scheelite, po=pyrrhotite, py=pyrite, gn=galena, sp=sphalerite, cpy=chalcopyrite, bn=bornite, witt=wittichenite, mo=molybdenite, gnbi=galenobismutite, bis=native bismuth, bin=bismuthinite, mc=marcasite, cc=chalcocite, cv=covellite

distribution of mineral assemblages which can be identified on the thin section, hand specimen, and deposit scales. These mineral associations, or characteristic assemblages of skarn formations at Tong Myeong mine are listed in Table 1 and described in the following paragraphs.

Skarns originated from crystalline limestone

Wollastonite skarn: This skarn occurs along the contact between the limestone and clinopyroxene-garnet skarn or garnet skarn. It is a few meter to a few centimeter in widths and contacts the limestone with a sharp boundary. Wollastonite skarn is composed chiefly of wollastonite with minor amounts of calcite, quartz, clinopyroxene, chlorite, garnet, and muscovite, but never contains scheelite or sulfide minerals. Wollastonite crystals are fibrous and tend to be perpendicular to the boundary with the limestone. They are rarely replaced by calcite and quartz.

Clinopyroxene skarn: Clinopyroxene skarn is dark green in color. The boundary between wollastonite and clinopyroxene skarn is sharp, but veinlets of wollastonite and clinopyroxene skarn are developed at the side of limestone. Clinopyroxene skarn is composed mainly of clinopyroxene, amphibole, and quartz with small amounts of garnet, vesuvianite, epidote, calcite, and scheelite.

Clinopyroxene and amphibole are euhedral to subhedral in shape, a few millimeters in size. The grain size is generally much finer in pyrrhotite-poor clinopyroxene skarn than in pyrrhotite-rich clinopyroxene skarn. The acicular amphibole in this skarn containing pyrrhotite is generally dark green, fine-grained, and randomly oriented. Clinopyroxene is partially converted to amphibole+quartz(±calcite). Most clinopyroxenes are filled with and/or cut by anisotropic garnet aggregates. In some cases, coarse grained garnet crystals contain very small inclusions of clinopyroxenes, suggesting that clinopyroxene and garnet are not deposited simultaneously. This fact indicates that fine-grained clinopyroxene is earlier than garnet.

In this skarn, scheelite occurs as fine-grained, subhedral to anhedral aggregates which appear to have grown contemporaneously with quartz.

Clinopyroxene-Garnet skarn: Clinopyroxene-garnet skarn is developed between clinopyroxene skarn and garnet skarn, and is gradually changed to garnet skarn. This skarn is composed of major clinopyroxene, amphibole, and garnet, and with minor amounts of quartz, calcite, epidote, chlorite, apatite. The relative abundance of clinopyroxene to garnet in this skarn is variable.

Clinopyroxene generally occurs as fine- to medium-grained and as anhedral to subhedral in shape, are partly altered to amphibole and chlorite. Locally, clinopyroxene is also partially replaced pseudomorphically by calcite. Clinopyroxene in this skarn is close to diopside in com position (about 90% diopside) (Oh and Park, 1983). The garnet which is reddish brown in color and ranges from very fine-grained anhedral aggregates to coarser-grained subhedra, generally displays weakly to strongly anisotropism showing slight optical zoning. Garnet is partly replaced, often pseudomorphically, by calcite, quartz, and sulfide minerals. Calcite is crystallized largely after the garnet and clinopyroxene. Quartz is generally present but normally in only minor amounts, replacing garnet or occuring interstitially to it.

Garnet skarn: Garnet skarn, which constitutes one of the largest skarn zones, is developed between clinopyroxene skarn or clinopyroxene-garnet skarn and wollastonite skarn. Also, garnet skarn is gradually changed to vesuvianite skarn. It is a dark reddish brown skarn consisting mainly of garnet. Accessory minerals are clinopyroxene, amphibole, calcite, chlorite, epidote, and quartz.

Euhedral to subhedral garnet ranges in size from 1mm to 1cm in diameter. Generally, garnet shows strong anisotropism with complex patterns of sector twinning or optical zoning.

Garnet core contain small euhedral inclusions of clinopyroxene, calcite, chlorite, and amphibole. These inclusions of clinopyroxenes are concentrated in the cores of the garnet crystals, suggesting that the clinopyroxenes were no longer formed in the final stages of growth of the garnet. Clinopyroxene are wholly or partially replaced by calcite and amphibole. The rim of garnet rarely contains some inclusions of scheelite. As noted by Oh and Park (1983), such zoned garnets commonly show an outward decrease in andradite to grossular ratio.

Often, this garnet skarns are crosscut by planar arrays of disseminated scheelite. Epidote is observed in garnet skarn as occuring interstitially to garnets.

In thin section, quartz and sulfides appear to replace interstitial garnet and clinopyroxene, probably indicating that they postdate the clinopyroxene.

Vesuvianite skarn: Vesuvianite skarn is developed between garnet skarn and hydrothermal vein. Vesuvianite skarn is composed chiefly of vesuvianite with minor amounts of chlorite, calcite, quartz, muscovite, clinopyroxene, garnet, and scheelite. The major differences in this skarn compared to other skarns are that vesuvianite, calcite, quartz, and pyrrhotite are much more abundant. Also, extensive development of chlorite-bearing vesuvianite skarn is particularly characteristic of Tong Myeong deposits. Vesuvianite grows as radiating or prismatic aggregates. Chlorite, muscovite, and calcite are common as replacements of vesuvianite.

In this skarn, scheelite is dominant ore mineral, but subordinate pyrrhotite may also be present. Scheelite occurs as coarser-grained, euhedral to subhedral in shape. Scheelite is found between vesuvianites as subhedral forms. This fact indicates that coarser-grained scheelite is earlier than vesuvianite.

Skarns originated from hornfels

Skarns originated from hornfels are restricted to relatively narrow areas in comparision with that from crystalline limestone.

These skarns are dark reddish brown in color, and sometimes preserve the well-developed bandings, suggesting the original structure of sedimentary rocks. They are mainly composed of clinopyroxene and garnet, and are accompanied by minor amounts of calcite, quartz, chlorite, amphibole, and muscovite. Because these skarns are extremely heterogenous, the zonation pattern

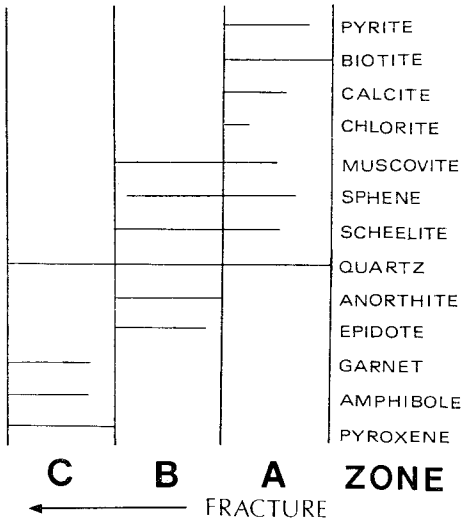

Fig. 1 Schematic diagram showing the paragenesis of skarns originated from hornfels at Tong Myeong mine, as developed adjacent to fractures and veinlets which cut the rock.

of these skarns are ambiguous and irregular. Garnet is generally fine-to medium-grained anhedral aggregates and optically isotropic to weakly anisotropic. Clinopyroxene occurs as pale green grains and is intimately associated with fine-grained amphibole.

On the scale of hand specimens and thin sections, a pattern of zonation of these skarn can sometimes be recognized bordering quartz-anorthite-bearing veins. These skarn can be subdivided into quartz-anorthite and clinopyroxene-amphibole-rich part. The former is composed of mainly quartz, anorthite, and muscovite with minor amounts of calcite, chlorite, clinopyroxene, amphibole, scheelite. The latter is composed chiefly of clinopyroxene and amphibole, accompanied by small amounts of epidote, muscovite, quartz,and calcite. The mineralogy and overall sequence of the skarn, as studied on a small scale, is shown in Fig. 1.

Alterations of igneous rocks

Two general types of hydrothermal alteration are observed in fine-grained biotite-hornblende granodiorite at Tong Myeong deposit: argillic—and prophylitic alteration. The periphery of igneous rocks is characterized by prophylitic and rare argillic alteration.

The argillic alteration occurs along the contact between the skarn bodies and igneous rocks. It is a narrow zone in widths, generally pale green in color. This argillic alteration is characterized by the complete replacement of plagioclase and mafic minerals by calcite, clay minerals, and sericite. A small quantities of pyrite occur as disseminates in altered plagioclase and mafic minerals.

The zone of prophylitic alteration surrounds the area of argillic alteration. Here the main alteration products are chlorite and albite. The feldspar is converted to sericite, with pyrite. This alteration zone are characterized by the chloritization of biotite and other mafic minerals along the cleavages.

ORE MINERALIZATION AND PARAGENESIS

The ore mineralogy of the Tong Myeong deposit is complex, but only a few minerals are

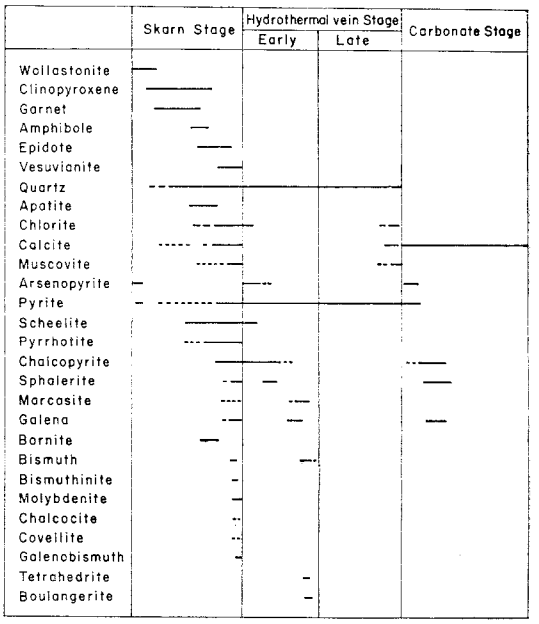

Fig. 2 The paragenetic sequences of ore minerals with skarn minerals.

widely formed in all mineralization stages. All of the ore minerals could be identified in polished sections. Pyrite and arsenopyrite are well observed in limestone. Minor pyrite and scheelite are sometimes developed along the fissures with in hornfels. The paragenetic sequences of ore minerals with skarns are shown in Fig. 2.

Skarn sulphides

The skarn contains pyrite, sphalerite, galena, pyrrhotite, marcasite, chalcopyrite, native bismuth, bismuthinite, galenobismutite, bornite, molybdenite, chalcocite, covellite, and scheelite. These minerals fill usually interstices to or rarely replace clinopyroxene and garnet. These ore minerals commonly occurr as fine disseminate or small masses in the calcic skarns. The predominant ore species among them is scheelite. Microscopic evidences suggest that these sulfide species are later than the skarn minerals.

Pyrite which is a common constituent of the skarn stage, is one of the earliest sulfide minerals to crystallize. Minor amounts of pyrite is that formed as an alteration product of older pyrrhotite. It occurs as coarse single crystals commonly containing microscopic relics of original pyrrhotite. It usually occurs as individual cubic crystal. Although present in small amounts, most sphalerite is pene-contemporaneous with pyrrhotite, chalcopyrite, and pyrite. This sphalerite during main sulfide stage is relatively iron-rich. Galena is generally rare, but is a common and widespread are mineral within the vesuvianite skarn. In that case, it is commonly associated with pyrrhotite and scheelite. Galena fill space between calc-silicates and scheelite crystals, and commonly replace pyrite and pyrrhotite. It is observed also locally within fractures cutting the pyrite and scheelite. Native bismuth, bismuthinite, and galenobismutite sometimes are associated with galena. Native bismuth also occur as patches and blebs in bornite-chalcopyrite assemblages, Chalcopyrite are widely distributed and evidently formed by varied mechanisms and at different times in paragenetic sequence. The chalcopyrite occurs: (1) as tiny veinlets in pyrite and replacement patches in pyrrhotite (2) as exsolution blebs in sphalerite (3) as coarse crystals intergrown with bornite. Pyrrhotite is a common constituent of the skarn, especially clinopyroxene-and vesuvanite skarn. A striking feature of the pyrrhotite is its widespread alteration, mainly to fine-grained "lamellar" pyrite and minor marcasite along the peripheries of the pyrrhotite grains and along fractures. In some specimens, these aggregates form perfect replacement of original pyrrhotite crystals. Bornite occurs as anhedral and is associated with chalcopyrite, native bismuth, bismuthinite, molybdenite, chalcocite, and covellite. Galena, pyrite, and sphalerite are completely absent in this ore specimen. Bornite contains spindlelike lamellae of chalcopyrite, probably of exsolution products, and is replaced by chalcocite and covellite along fractures.

Hydrothermal veins

Pyrite is the predominant sulfide species in all the vein mineral of the studied area, associated with minor scheelite, sphalerite, galena, aresenopyrite, chalcopyrite, marcasite, native bismuth, tetrahedrite, and boulangerite. Hydrothermal vein stage may be divided broadly into the following two stages on the basis of their field occurrences, hand specimens, and mineral assemblages.

Early vein stage: TheW-mineralization during early vein stage is the predominant one in this mine. Quartz, the most abundant gangue mineral, is massive in appearance and is usually white to gray in color. This stage is characterized by the following ore minerals.

Pyrite is a common constituent of the veins, and frequently as aggregates of sub- to anhedral grains which are intimately intergrown with marcasite. Most arsenopyrites are observed within the vein, evidently overlapping pyrite and scheelite. Arsenopyrite occurs as euhedral grains.

Minute inclusions of pyrrhotite in arsenopyrite might suggest continued deposition of arsenopyrite after pyrrhotite, but no veinlets of arsenopyrite cutting pyrrhotite were observed. Chalcopyrite is distributed irregularly throughout the vein as small anhedral mass. It occurs also locally within fractures cutting the pyrite and forms as coarse crystals intergrown with galena, tetrahedrite, boulangerite. Chalcopyrite is commonly found in association with sphalerite as dispersed spots visible to the naked eye, but the two minerals also frequently exhibit exsolution textures. Sphalerite showing red internal reflections, occurs as coarse crystals intergrown with pyrite. Galena, which occurs as subhedral fine grains, is rarely formed associated with native bismuth, bismuthinite, sphalerite, chalcopyrite, and pyrite. Native bismuth is closely associated with boulangerite and tetrahedrite, forming isolated replacement patches in early galena.

Late vein stage: Mild brecciation of early veins preceded and late vein stage minerals fill usually interstitial to early vein quartz. These veins formed during late vein stage are composed of clear quartz, calcite, chlorite, white micas, and pyrite.

Clear quartz is the most abundant gangue mineral. Euhedral clear quartz occurs often as druses. Prolific development of white micas is commonly observed as products of precipitation within the veins themselves. Pyrite occur as small amounts of euhedral grains in vugs.

Carbonate stage

The latest phase of tectonic activity occurred after mineralization of the hydrothermal vein stage. Post-ore faults have been filled with calcite and minor amounts of arsenopyrite, pyrite, sphalerite, galena, and chalcopyrite. Calcite occurs in two distinctive color which always exhibit the same paragenetic sequence: milky white and pinkish calcite. A pinkish calcite occurs well developed rhombohedral crystals, but milky white calcite occurs always as aggregates of anhedral grains. Milky white calcite precipitation is partially overlapped sulfide precipitation. Pyrite occurs as euhedral grains with cube and pyritohedron. Galena is present as small, well cleaved masses, as well as in crystallized mixtures with sphalerite and pyrite. Sphalerite commonly contains oriented rows of chalcopyrite blebs, caused sometimes by the result of exsolution.

SCHEELITE MINERALIZATION

Scheelite distribution

Almost all the tungsten mineral in Tong Myeong deposit occurs as scheelite. Scheelite is widely distributed in clinopyroxene to vesuvianite skarn and, also in quartz veins, hornfels, and acidic igneous rocks near the skarn bodies, but not in limestone and wollastonite skarn. It is fine grained in clinopyroxene, clinopyroxene-garnet, and garnet skarn but relatively coarse grained in vesuvianite skarn and in quartz veins.

The patches of garnet skarn are crosscut by planar arrays of disseminated scheelite. Scheelite is most concentrated in the vesuvianite skarn, where it occurs as coarser euhedral to subhedral grains associated with pyrrhotite in fine-grained coatings on vesuvianite skarns. Scheelite grains associated with vesuvianite are generally large and euhedral, which show commonly pale blue fluorescence under short ultraviolet radiation. This indicates that scheelite are nearly pure $CaWO_4$ as compared to fine-grained scheelites in clinopyroxene-and garnet skarn, which locally exhibits light yellow fluorescene color indicating the presence of molybdenum content (Greenwood, 1943; Shoji and Sasaki, 1978; So and Park, 1979).

Scheelites in the various skarns are mainly crystallized at an late period of skarn stage, whereas the mineral in quartz veins have formed early period of hydrothermal stage. The precipitation of scheelite may be continued during the entire period ranging from skarn stage to early

hydrothermal stage.

Scheelite deposition

Hochella et al. (1982) suggests that the thermal stability of vesuvianite is greatly shifted toward lower temperatures by the presence of quartz. The equilibrium temperature for the stability of vesuvianite+quartz was located at 388°±10°C at 1 kb and 405°±5°C at 2 kb Pfluid

A variations in pH may have played determ--ining roles. Indeed, these factors may have been interrelated through the increased dissolution of calcite with increased acidity, although this effect is probably significantly reduced at temperatures in excess of 400°C (Holland and Malinin, 1979), such as

$$CaCO_3+2H^+ \longrightarrow Ca^{+2}+H_2CO_3$$

prevailed during early skarn formation. As inferred on experimental grounds by Wesolowski et al. (1982). Typical tungsten-rich ore solutions (T=300°−500°C) is transported as HWO_4^-, so that scheelite deposition would occur in response to an increase in pH.

The correlation between pyrrhotite and scheelite implies that a critical factor in the formation of this unusually rich orebody may have been pH changes stimulated by such reactions (Barnes, 1979):

$$FeCl_2aq+H_2S\ aq \longrightarrow FeS(\text{pyrrhotite})+2H^++2Cl^-$$

The release of H^+ would enhance calcite dissolution. Thus, pH is increased in the fluid, leading to scheelite deposition.

Hsu and Galli (1973) and Hsu (1977) conclude that an oxidized environment favors the formation of $CaMoO_4$-rich scheelite, whereas a reduced one results in purer scheelite with molybdenite. Scheelite at Tong Myeong mine is generally free from molybdenum because of the blue fluorescent color. The formation of highly pure scheelite could have resulted from the reduced environment.

The size, shape, and fluorescent color of scheelite associated with vesuvianite suggest that the scheelite was precipitated during retrograde alteration.

REFLECTION-MICROHARDNESS CHARACTERISTICS OF THE ORE MINERALS

Instrumentation

Microphotometer system: Reflectivity measurements in the present study were made using an RCA type 1P21 photomultiplier, used in conjunction with a Leitz ORTHOLUX microscope, accurately adjusted to give normally incident plane polarized light. The light source for all observations was a 12 volt 100 watt halogen lamp, operating at a color temperature of about 3,400°K. To avoid fluctuations in light intensity, the applied voltage was stabilized by a constant voltage transformer by Knott Electronik, Munich. The output from the responding photomultiplier being recorded on a spot galvanometer (NORMA) of 2K ohms internal resistance and full scale deflection of 0.0018uA on its most sensitive scale.

The resulting light intensity and the sensitivity of the photomultiplier were sufficient to allow monochromatic determinations to be made by interposing a series of Leitz interference filters of a half-value width of about 200A° and of a maximum transparency of about 60%, between the light source and vertical illuminator tube. All determinations were made under X20, 0.40 N.A. in air and X50, 0.85N.A. in oil, strain-free objectives, carefully centered.

Microhardness tester: The microhardness equipment used for this study is the MINILOAD hardness tester, manufactured by E. Leitz, Ltd., Wetzlar, for determining Vickers Hardness Number (VHN) by making four-sided diamond shaped pyramidal indentation in the polished mineral surface. The indenter can be applied to mineral grains as small as 2∼3 micron in diam-

eter and each pair of opposed faces makes an angle of 136°. The diagonal of the resulting microindentation is about seven times the depth of penetration. The rate of loading is controlled by means of a small hydraulic damper.

Standard

Since the widely used methods of reflectance measurement depend on direct comparison of the unknown with a standard of known reflectance, accurate and reliable standards are of the utmost importance. The number of these standards will vary according to the characteristics of the equipment. Ideally, for general acceptance, such standards should be isotropic, show little spectral dispersion of reflectivity, be hard, opaque and homogeneous, easily reproducible and permanent. Such severe requirements are very difficult to fulfill in practice.

The standards employed in the present study are WTiC 260 which possesses spectral dispersions of 44.5 to 50.3% in air and SiC 290 which possesses spectral dispersions of 20.5 to 22.8% in air, at wavelengths of 403nm to 615nm. The relative standard deviation referred to the mean reflectance at a given wavelength is ± 1.5%.

Accuracy

Gray and Millman (1962) suggested that the accuracy of the reflectivity measurements varies between ± 1/2 to 2% of the measured value and is dependant on spectral wavelength and the general order of reflectivity under the most standard conditions. Both in the reflectivity and microhardness measurements of this study, there are errors caused by leveling, focusing and due to setting of microscope and also errors caused by the specimen. The total relative error of reflectivity measurements varies within ± 0.7 depending on spectral wavelengths at a flawless surface under standard conditions. Green, blue and yellow measurements are usually subject to the lower values of the range of errors, and the measurements in violet and orange wavelengths to the highest part of the range. Mitsche and Onitsch(1951) have shown a gradual increase in indentation size with time, and standardization of the contact time is obviously desirable. The time of the indentation procedure was not kept constant, 15~20sec. The relative error of Miniload aganist the mean microhardness value of a hardness test plate and a test certificate by MPA Dortmund is ± 1.0% at 100g and ± 1.5 % at 15g.

Results

Reflectance variation of bireflecting sulfide species: The reflectance of nine studied sulfides were measured on the unoriented sections. All reflectance values for the studied mineral species are summarized in Table 2.

Anisotropic minerals are bireflecting except for section at 90° to the optic axis in case of uniaxial minerals, sections of these minerals show a range of reflectance value defined by spectral profiles. All reflectance value of skarn-and hydrothermal stage anisotropic minerals measured in air and oil, are shown graphically in Fig. 3 and 7.

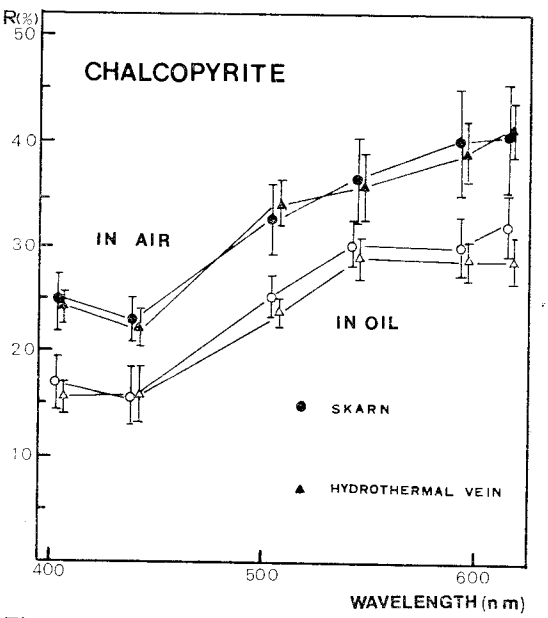

Fig. 3 Spectral profiles for chalcopyrite of different mineralization stage measured in air and oil.

Table 2 Spectral reflectances (R%) of the studied anisotropic mineral species for different mineralization stages in air and oil.

Mineralization Stage	Mineral Studied	Sample No.	403(violet)		438(indigo)		504(blue)		544(green)		593(yellow)		615(red)	
			air	oil	air	oil	air	oil	air	oil	air	oil	air	oil
Skarn Stage	Bornite	DM039	12.7	4.0	13.1	4.6	12.5	5.0	13.3	5.0	16.7	8.1	19.7	10.0
			15.0	4.9	15.9	5.8	15.1	6.0	16.6	5.9	20.8	8.5	23.5	11.4
			11.8	4.0	13.1	4.0	12.8	4.9	13.2	5.6	16.1	8.0	19.0	10.7
			15.1	4.7	16.0	5.0	16.0	5.7	17.2	6.1	21.6	8.7	24.3	12.1
			14.0	4.2	14.7	4.6	14.0	4.8	14.9	5.3	17.6	7.8	20.5	10.8
			15.2	4.9	16.0	5.5	15.4	5.7	16.8	5.6	20.7	8.3	23.9	11.6
		Mean	12.8	4.1	13.6	4.4	13.1	4.9	13.8	5.3	16.8	8.0	19.7	10.5
			15.1	4.8	16.0	5.4	15.5	5.8	16.9	5.9	21.0	8.5	23.9	11.7
	Chalcopyrite	DM039	22.0	14.3	20.6	13.1	29.5	23.2	31.9	27.0	35.4	27.1	35.0	29.9
			26.8	18.9	24.9	17.8	34.0	25.3	37.9	29.2	43.8	31.2	43.9	34.8
			21.4	15.0	20.9	13.9	30.0	23.8	33.5	27.5	36.7	27.7	35.0	31.9
			28.9	19.7	25.7	18.2	37.9	27.5	42.4	31.9	48.8	33.1	46.8	37.4
		DM026	22.3	13.9	21.1	12.1	28.8	23.1	31.7	30.2	33.2	27.2	36.2	26.0
			26.8	19.7	24.7	19.2	35.9	29.0	40.3	36.9	42.8	34.9	45.8	33.0
		Mean	21.9	14.4	20.9	13.0	29.4	23.4	32.4	28.2	35.1	27.3	35.4	29.3
			27.5	19.4	25.1	18.4	35.9	27.3	40.2	32.7	45.1	33.1	45.5	35.1
	Molybdenite	DM039	17.7	7.8	19.3	8.6	18.2	9.0	16.2	8.1	19.0	7.0	19.2	6.0
			27.8	17.8	36.7	19.8	30.0	19.6	24.1	17.9	26.8	19.2	26.9	15.6
			15.8	6.0	17.0	7.3	16.1	5.9	20.5	4.7	16.9	4.7	16.2	5.5
			31.1	10.1	35.8	17.1	26.3	15.2	29.2	14.0	27.9	14.3	26.1	16.8
		Mean	16.8	6.9	18.2	8.0	17.2	7.5	18.4	6.4	18.0	5.9	17.7	5.8
			29.5	14.0	36.3	18.5	28.2	17.4	26.7	16.0	27.4	16.8	26.5	16.8
	Pyrrhotite	DM026	27.3	14.1	26.7	13.8	31.0	15.9	29.6	19.1	31.9	20.0	34.0	19.9
			32.1	19.4	31.9	20.7	38.1	20.7	37.0	23.7	40.1	24.2	41.1	26.1
			28.1	14.0	28.0	14.1	30.0	16.2	29.6	18.1	31.2	17.5	31.8	18.0
			32.4	19.3	32.6	19.9	37.0	21.4	37.0	24.0	39.4	23.7	38.9	24.7
		DM 021-1	30.4	14.4	31.0	13.9	33.0	17.0	34.5	19.1	38.8	19.9	39.4	22.6
			34.1	19.8	34.6	20.9	38.3	25.4	38.5	27.1	42.1	28.2	42.4	30.5
		DM030	27.0	15.0	26.0	15.6	29.9	19.0	32.0	21.7	33.9	23.0	34.9	23.7
			31.9	18.0	32.1	19.6	36.1	22.8	37.0	24.3	40.0	25.7	40.7	27.0
			27.8	16.0	27.2	15.7	29.8	20.1	30.2	21.9	34.0	24.0	34.9	26.2
			32.2	19.8	32.9	19.5	36.2	22.9	37.2	24.8	39.8	26.2	40.9	29.0
		Mean	28.1	14.7	27.8	14.6	30.7	17.6	31.2	20.0	34.0	20.9	35.0	22.1
			32.5	19.3	32.8	20.1	37.1	22.6	37.3	24.8	40.3	25.6	40.8	27.5
	Galenobismutite	DM21-1	38.2	20.4	36.8	19.9	33.4	21.6	31.5	19.5	31.1	18.2	30.2	19.0
			50.4	32.9	48.3	32.6	45.0	31.6	44.1	29.3	44.3	27.2	44.3	29.1
			38.0	20.3	37.1	20.1	34.9	21.9	32.5	19.6	32.0	19.1	31.4	20.1
			49.8	33.8	47.8	32.1	45.5	31.5	42.8	29.3	44.1	28.3	43.9	29.2
		Mean	38.1	20.4	37.0	20.0	34.2	21.8	32.0	19.9	31.6	18.7	30.8	19.6
			50.1	33.4	48.1	32.4	45.3	31.6	43.5	29.3	44.2	27.8	44.1	29.2
Hydrothermal vein stage	Arsenopyrite	DM 016-1	42.8	28.8	42.4	23.6	45.0	28.3	42.9	28.0	43.7	29.5	44.0	29.6
			47.3	35.9	48.6	36.5	52.2	36.0	51.2	38.2	52.2	34.9	52.2	35.7
			39.9	28.1	41.5	25.9	43.5	31.2	42.7	27.4	43.5	29.3	44.0	29.9
			46.2	34.4	48.3	35.0	51.2	39.1	51.1	36.8	51.0	37.9	51.0	38.8
		Mean	41.4	28.5	42.0	24.8	44.3	29.8	42.8	27.7	43.6	29.4	44.0	29.8
			46.8	35.2	48.5	35.8	51.7	37.6	51.2	37.5	51.6	36.4	51.6	37.3
	Chalcopyrite	DM 016-1	23.0	13.0	22.0	13.1	32.8	21.7	33.2	27.2	37.2	27.7	39.1	25.0
			26.1	15.8	24.0	18.9	36.7	24.7	38.3	31.2	42.1	31.0	43.1	31.0
			22.1	15.0	21.0	13.4	31.2	23.0	32.0	27.0	35.4	26.1	38.0	28.0
			25.0	18.0	23.9	18.0	36.0	25.4	39.0	30.7	41.8	30.2	44.3	31.1

	Mean	22.6	14.0	21.5	13.3	32.0	22.4	32.6	27.1	36.3	26.9	38.6	26.5
		25.6	16.9	24.0	18.5	36.4	25.1	38.7	31.0	42.0	30.6	43.7	31.1
Marcasite	DM	42.0	19.5	44.0	22.5	45.0	29.0	43.2	34.9	45.0	31.3	46.5	32.8
	016-1	44.3	27.0	46.7	32.4	47.3	38.1	50.3	40.1	51.0	37.5	52.4	38.3
		43.1	18.1	45.0	22.1	44.9	28.0	41.9	32.2	48.0	27.8	49.0	27.5
		45.8	29.0	48.0	34.1	47.8	36.8	49.8	39.0	51.3	35.9	51.2	36.0
	Mean	42.6	18.8	44.5	22.3	45.0	28.5	42.6	33.6	46.5	29.6	47.8	30.2
		45.1	28.0	47.4	33.3	47.6	37.5	50.1	40.0	51.2	36.7	51.8	37.2
Boulangerite	DM	39.7	24.5	39.8	25.4	36.3	24.2	37.2	24.5	37.1	23.1	36.0	23.0
	016-1	48.7	31.2	45.2	28.7	43.5	27.3	44.9	27.4	43.0	26.0	41.8	27.2
		39.4	25.4	38.8	24.9	34.5	23.2	37.0	24.1	37.3	21.5	35.3	23.1
		49.3	30.9	45.7	29.8	44.5	28.3	44.8	29.0	43.2	27.5	41.1	28.8
		39.1	25.1	38.0	24.7	33.5	22.5	34.8	23.0	34.9	22.1	33.7	23.0
		48.1	30.2	45.1	29.0	42.4	27.1	42.6	26.9	41.0	26.0	40.1	26.0
	Mean	39.4	25.0	38.9	25.0	34.8	23.3	36.3	23.9	36.4	22.2	35.0	23.0
		48.7	30.8	45.3	29.2	43.5	27.6	44.1	27.8	42.4	26.5	41.0	27.3
Tetrahedrite	DM	29.2	13.0	29.0	14.9	30.1	16.0	31.3	15.2	31.0	15.3	30.5	14.9
	016-1	30.1	14.5	29.9	16.0	32.0	16.3	32.8	16.0	32.6	16.2	32.0	16.0
		29.1	13.9	29.0	14.5	30.0	15.8	30.2	14.1	30.0	15.4	30.1	15.0
		30.2	14.3	30.0	15.9	31.8	16.1	32.1	16.0	31.9	16.0	32.0	16.0
	Mean	29.2	13.5	29.0	14.7	30.1	15.9	30.8	14.7	30.5	15.4	30.3	15.0
		30.2	14.4	30.0	16.0	31.9	16.2	32.5	16.0	32.3	16.1	32.0	16.0

In Fig. 3. chalcopyrite, skarn-and hydrothermal vein stage, represents steeply progressive increase in reflectance until red wavelengths, showing a slight depression around 438nm in the profiles. Skarn stage chalcopyrite has slightly higher reflectance value than hydrothermal vein stage chalcopyrite at 544nm. Skarn stage chalcopyrite indicate more strong bireflectance at each wavelength than hydrothermal vein chalcopyrite.

Bornite, pinkish brown in white light, shows gently progressive increase toward red wavelengths, showing the weakest bireflectance at each

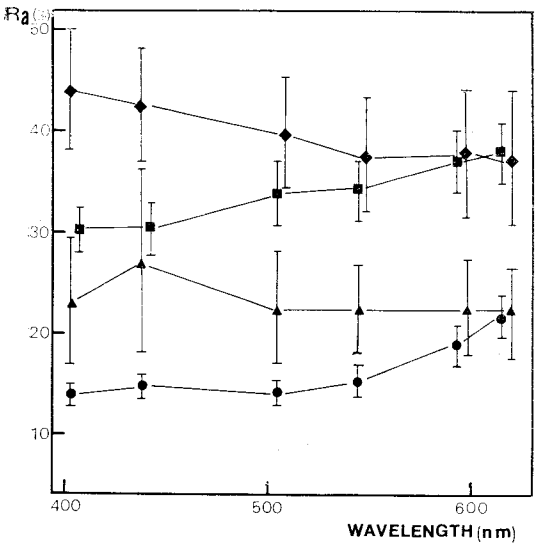

Fig. 4 Spectral profiles of skarn stage minerals measured in air. (solid circle: bornite; solid triangular: molybdenite; solid square: pyrrhotite; solid rhombus: galenobismutite)

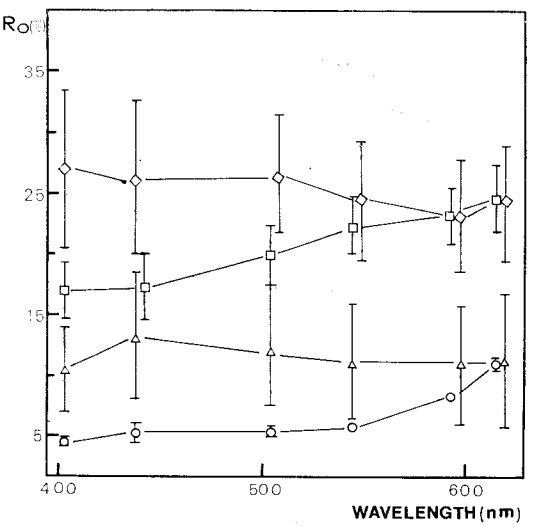

Fig. 5 Spectral profiles of skarn stage mineral species measured in oil. (open circle: bornite; open triangular: molybdenite; open sqare: pyrrhotite; open rhombus: galenobismutite)

wavelength. Molybdenite, with relatively flat profiles, appears whitish to gray in white light illumination and indicates the strongest bireflectance at each wavelength. Pyrrhotite, creamy pinkish brown under the microscope, represents a little steep profiles and showing a progressive increase in reflectivity towards red wavelength. Galenobismutite, with very strong bireflectance, represents relatively progressive increase in reflectivity towards red wavelength (Fig. 4 and 5).

Arsenopyrite, white with pale-creamy in white light, presents progressive increase in reflectivity towards red wavelength, but showing a pronounced dip around blue-green wavelength in air and oil. Also, arsenopyrite are represented by broad depressions in the profiles. Marcasite, pale yellow in color, shows a steeply progressive increase until green wavelength in oil, showing a absorption band at 593nm. Boulangerite, a dull gray in white light, represents a little steep profiles and showing a progressive decrease in reflectivity towards red wavelengths, and indicates the strong bireflectance at each wavelength. Tetrahedrite, gray with brownish tint under the microscope, represents a gently progressive increase toward red wavelength in air and oil (Fig. 6 and 7).

The reflectance variation depending on paragenetic sequence may be resulted from variation of structure and composition due to different physicochemical conditions in time during the skarn and hydrothermal system.

Effect of internal reflection power of sphalerite on its reflectances: The studied sphalerite shows yellow-and red-colored internal reflection, under crossed nicols, due to variation of chemical impurities. The visibility of internal reflections are also enhanced by using oil immersion objectives. The intensity and nature of the colors vary from white to pale amber in low iron manganese varieties through various shades of red to deep ruby as iron and/or manganese

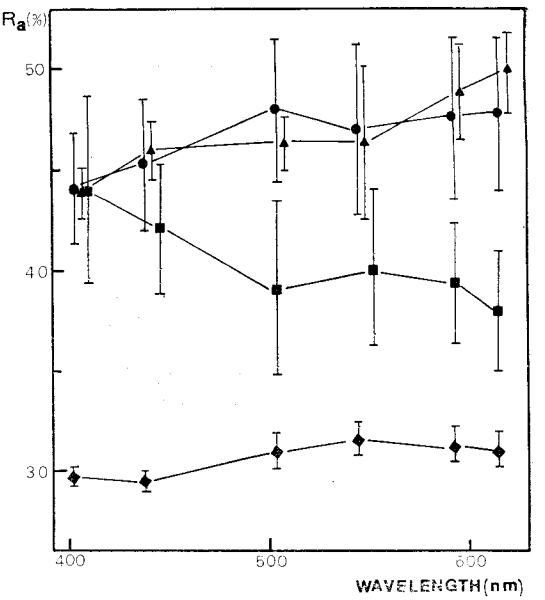

Fig. 6 Spectral profiles of hydrothermal vein stage minerals measured in air (solid circle: arsenopyrite;solid triangular: marcasite; solid square: boulangerite; solid rhombus: tetrahedrite)

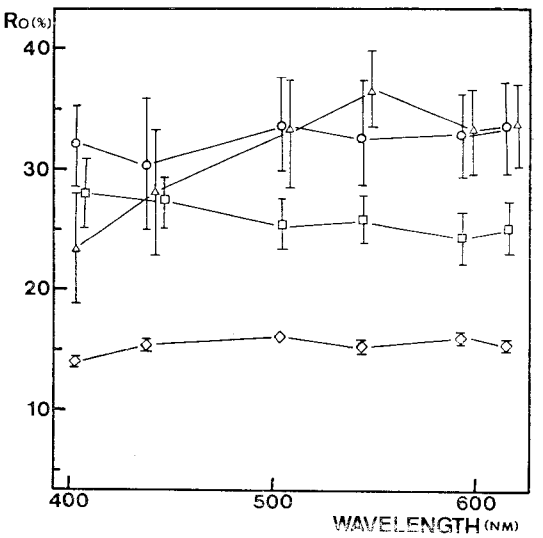

Fig. 7 Spectral profiles of hydrothermal vein stage minerals measured in oil. (open circle: arsenopyrite; open triangular: marcasite; open square: boulangerite; open rhombus: tetrahedrite)

increase. Consequently, sections of the sphalerites with internal reflection show a range of reflectivity, resulting in sympathetic variation in the shape of profiles (So, 1984). At about 10

Table 3 Reflectances(%) of sphalerite (in air and oil) with different internal reflection colors.

Color	Sample No.	403(violet)		438(indigo)		504(blue)		544(green)		593(yellow)		615(red)	
		air	oil	air	oil	air	oil	air	oil	air	oil	air	oil
Yellow	DM016-2	16.5	5.5	17.9	5.0	17.1	5.8	16.0	5.0	15.9	6.2	16.3	6.0
		16.8	6.0	18.2	6.5	17.5	6.0	16.3	5.5	16.1	6.5	16.5	6.5
	DM016-3	18.4	5.8	16.3	4.9	15.6	4.8	15.3	4.6	15.1	4.5	15.0	4.5
		19.0	6.0	17.0	5.2	16.5	5.0	16.2	5.0	16.0	5.0	15.9	5.4
	Mean	17.5	5.7	17.1	5.0	16.4	5.3	15.7	4.8	15.5	5.4	15.7	5.3
		17.9	6.0	17.6	5.9	17.0	5.5	16.3	5.3	16.1	5.8	16.2	6.0
Red	DM016-3	18.0	5.7	16.2	3.8	15.8	4.6	16.0	4.2	15.3	4.1	15.2	4.3
		19.0	6.0	17.2	4.0	16.8	4.7	17.1	4.5	16.5	4.5	16.5	4.6
		18.3	5.9	16.6	3.5	16.2	4.8	15.6	4.3	15.1	4.2	15.0	4.6
		19.0	6.2	17.3	4.0	17.0	4.9	16.6	4.6	16.1	4.5	16.0	4.7
	Mean	18.2	5.8	16.4	3.6	16.0	4.7	15.8	4.3	15.2	4.2	15.1	4.5
		19.0	6.1	17.3	4.0	16.9	4.8	16.9	4.6	16.3	4.5	16.3	4.7

percent Fe the mineral becomes opaque, and internal reflections can no longer be observed (stanton, 1972).

First a portion of the polished section of the sphalerite specimen was chosen, where the internal reflection could be only observed under crossed nicols, but the reflectivity was measured under parallel nicols in air and oil. The results are presented in Table 3.

The reflectivity of the portion which showed internal reflection only between crossed nicols was in full agreement with normal values of the sphalerite in air. On the other hand, the reflectivity values which shows yellow internal reflection were higher than the normal values without internal reflection in oil. Also, spectral dispersion of sphalerite showing red internal reflection under crossed nicols, has lower values than the normal values without internal reflection (Fig. 8).

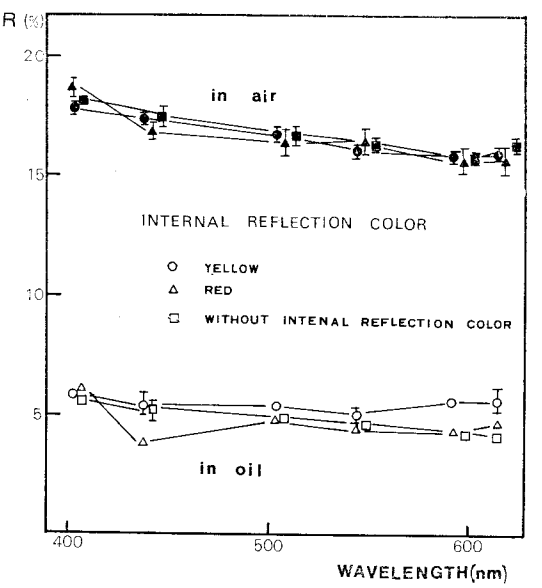

Fig. 8 Spectral dispersion of sphalerite with various internal reflection color, measured in air and oil, compared to those not showing internal reflection.

Determination of optical symmetry of the sulfides: The optical symmetries of many aniso tropic ore minerals can be partly or wholly determined from reflectivity measurements in monochromatic light, and that the usefulness of reflectivity data in identification of ore minerals can thereby be greatly increased (Cameron, 1963). Reflectivity data for the four bireflecting minerals studied are given in Table 4 and Fig. 9.

Each line represents, to scale, the bireflectance of a single mineral grain. The end points of the line give the values of Re′ and Rw for the grain.

In uniaxial mineral, the high values (w ray) for all grains are the same within the error of measurement, whereas the low values (e′ ray) are difficult for different grains. In this case the

Tabla 4 Reflectivity measurements of the studied chalcopyrite, marcasite, arsenopyrite and bornite at 544nm.

Grain	Chalcopyrite		Marcasite		Arsenopyrite		Bornite	
	Re′	Rw	Re′	Rw	Re′	Rw	Re′	Rw
1	29.0	36.1	47.0	51.0	44.5	50.1	17.9	22.8
2	29.0	36.9	48.5	51.1	43.1	49.9	18.0	22.0
3	28.5	39.4	46.4	50.1	43.7	49.6	18.8	23.0
4	28.0	39.0	48.7	50.0	45.0	52.1	18.5	21.1
5	35.6	38.4	47.0	53.0	45.4	51.8	19.5	22.0
6	34.7	38.9	46.3	51.0	43.7	50.3	18.1	21.0
7	21.7	37.6	47.8	51.0	44.5	51.7	18.8	20.7
8	21.2	38.4	49.0	51.1	42.7	49.8	18.0	20.9
9	28.0	37.2	47.0	51.0	43.7	52.0	17.4	20.3
10	28.8	38.0	45.2	50.7	43.0	51.3	17.6	20.1
11	31.5	36.4	49.8	53.2	43.9	51.2	15.7	19.6
12	31.9	37.9	47.8	50.5	43.0	49.7		
13	33.5	42.4	48.5	51.1	42.9	51.2		
14	31.7	40.3	43.2	50.3	42.7	51.1		
15	33.2	38.3	41.9	49.8				
16	32.0	39.0						
Rm	35.9		49.8		47.3		19.6	
Optic sign	−		−		intermediate		+	

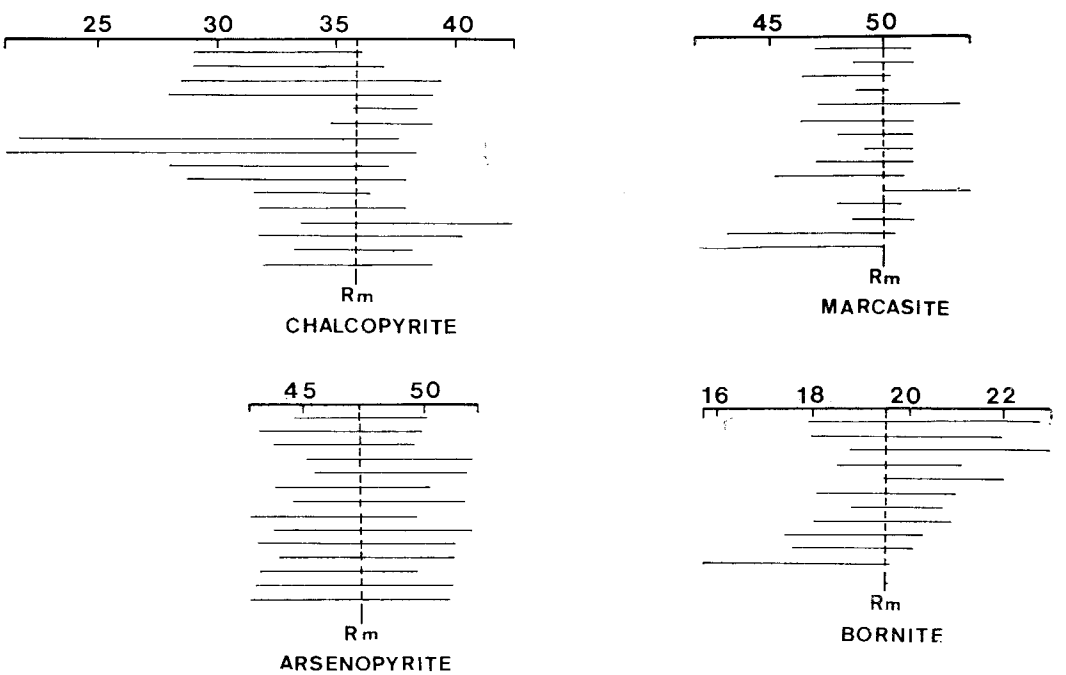

Fig. 9 Reflectances of diversely oriented grains of chalcopyrite, marcasite, arsenopyrite and bornite. Scale give reflectivity in percent.

mineral is uniaxial negative. Also, the low values are the same, the high values differ, and the mineral is uniaxial positive. But, in present study, the measurements indicate that for none of the minerals is Re′ or Rw constant, and that the minerals cannot be uniaxial.

Chalcopyrite(16 grains) indicates that they give non-uniaxial character, and show a value of Re′ that is less than 35.9 and a value of Rw that is greater than 35.9. This value was taken as the Rm value. The Rm value is clearly closer to the maximum value for the mineral (Rw) than to the minimum value(Re′); chalcopyrite can be indicated as optically negative. Marcasite shows a value of Re′≦49.8 and Rw≧49.8. Therefore, the Rm value is 49.8 and is closer to the maximum value(Rw) than to the minimum value(Re′); the optic sign is negative. For bornite, the value of Rm lies between 19.5 and 19.6; the indicated optic sign is positive. For arsenopyrite, Rm-Re′ is approximately equal to Rw-Rm, hence the optic sign is indeterminate within the limits of errors.

Microhardness variation of bireflecting sulfide species: Isotropic minerals of essentially constant composition give reasonably useful values. On the other hand, members of isomorphous series, or minerals which have limited compositional variations in solid solution, show variations which are thought to be due, in part, to the variable composition. Bireflecting minerals may show marked differences in hardness with respect to the orientation of the indentation with the crystallographic axes (Robertson and Meter, 1951). The indentation characteristics and vickers hardness values were studied at the same point at which the reflectivity was measured, by applying various testing loads ranging from 25 to 300 grams. Results are presented in Table 5 and Fig. 10-12.

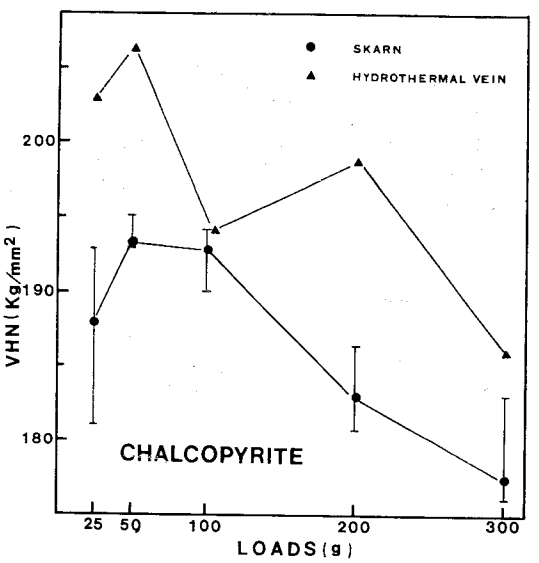

Fig. 10 Vickers hardness number for chalcopyrite of different mineralization stage.

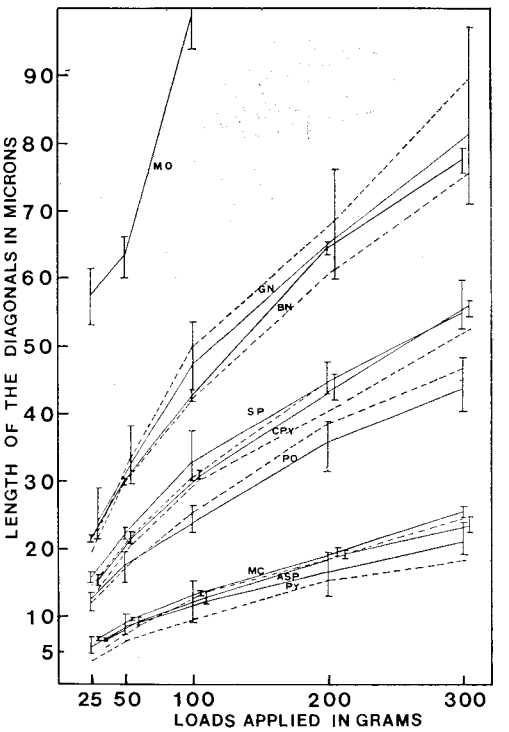

Fig. 11 The length variation of diagonals from Vickers indentation on the sulfides studied with various test loads (solid line: data from present study; dashed line: data from Nakhla, 1956). PY=pyrite, ASP=arsenopyrite, MC=marcasite, PO=pyrrhotite, SP=sphalerite, CPY=chalcopyrite, BN=bornite, GN=galena, MO=molybdenite. Symbols are same subsequently in diagrams.

Table 5 Vickers microindentation hardness measured for anisotropic minerals of the different mineralization stage.

Mineralization Stage	Minerals Studied	Sample No.		Weights applied in grams					Mean Value
				25	50	100	200	300	
Skarn Stage	Bornite	DM039	m	21.1 21.5	29.5 29.5	42.3 41.8	64.6 63.7	77.4 75.8	99.63
			VHN	102.18	106.54	104.63	89.98	94.81	
			m	22.1 22.1	30.0 30.4	43.2 43.6	64.9 65.6	77.6 79.4	93.94
			VHN	94.92	101.66	98.45	84.37	90.28	
		Mean	m	21.6 21.8	29.8 30.0	42.8 42.7	64.8 64.7	77.5 77.6	96.82
			VHN	98.45	103.71	101.23	88.32	92.38	
	Chalcopyrite	DM039	m	15.3 15.6	20.9 22.7	30.3 31.4	43.7 45.5	54.9 55.9	190.00
			VHN	192.97	195.10	194.22	186.45	181.26	
			m	16.3 15.6	21.9 21.8	31.7 30.6	45.9 44.7	55.3 57.0	184.36
			VHN	181.09	193.32	190.50	180.73	176.14	
		Mean	m	15.8 15.6	21.4 22.3	31.0 31.0	44.8 45.1	55.1 51.5	187.24
			VHN	188.08	193.32	192.96	183.15	178.67	
	Molybdenite	DM039	m	61.5 53.2	66.3 60.2	94.0 103.3	139.8 140.2	180.4 173.0	18.60
			VHN	14.07	23.14	19.04	18.92	17.82	
	Pyrrhotite	DM026	m	13.4 13.5	17.3 17.5	25.0 26.1	35.1 36.9	43.6 45.0	282.65
			VHN	254.38	306.25	282.96	286.17	283.48	
			m	12.5 12.3	17.1 17.4	25.0 25.2	34.9 35.1	43.6 44.4	299.15
			VHN	301.51	309.80	294.34	302.76	287.36	
		DM021-1	m	13.5 13.0	19.6 19.0	26.6 26.5	38.5 37.7	48.5 48.0	253.41
			VHN	262.08	248.91	262.08	255.50	238.47	
		DM030	m	13.6 12.4	19.2 17.4	26.1 24.0	38.9 35.1	45.4 40.5	283.46
			VHN	274.32	276.87	294.34	270.91	300.88	
			m	11.4 10.9	16.7 16.2	24.3 22.5	34.2 31.5	42.1 40.2	343.84
			VHN	369.58	340.57	338.67	342.64	327.74	
		Mean	m	12.9 12.4	18.0 17.5	25.4 24.9	36.3 35.3	44.6 43.6	289.50
			VHN	287.43	292.64	292.01	289.38	286.05	
Hydrothermal vein stage	Arsenopyrite	DM016-1	m	6.8 6.5	9.2 8.9	12.1 12.7	18.8 19.7	23.9 22.6	1075.77
			VHN	1032.75	1119.67	1206.04	995.68	1024.73	

		m	6.5 6.9	8.8 9.9	12.4 13.9	18.9 19.9	25.0 25.0	1004.38
		VHN	1032.75	1049.34	1064.28	985.44	890.11	
	Mean	m	6.7 6.7	9.0 9.4	12.3 13.3	18.9 19.8	24.5 23.8	1039.09
		VHN	1032.75	1095.46	1131.84	985.44	949.94	
Chalcopyrite	DM016-1	m	14.7 15.5	21.5 20.9	30.7 31.0	44.2 42.2	54.9 54.4	197.70
		VHN	203.32	206.30	194.22	198.73	185.94	
Marcasite	DM016-1	m	6.7 7.0	9.5 10.0	13.1 14.0	19.8 20.2	25.0 26.5	940.95
		VHN	973.75	965.43	1002.60	927.2	835.77	
		m	7.1 6.5	10.0 9.5	13.5 13.7	19.2 20.4	26.0 26.4	945.42
		VHN	1002.60	965.43	1002.60	946.03	810.44	
	Mean	m	6.9 6.8	9.8 9.8	13.3 13.9	19.6 20.1	25.5 26.5	940.26
		VHN	973.75	965.43	1002.60	936.54	822.96	

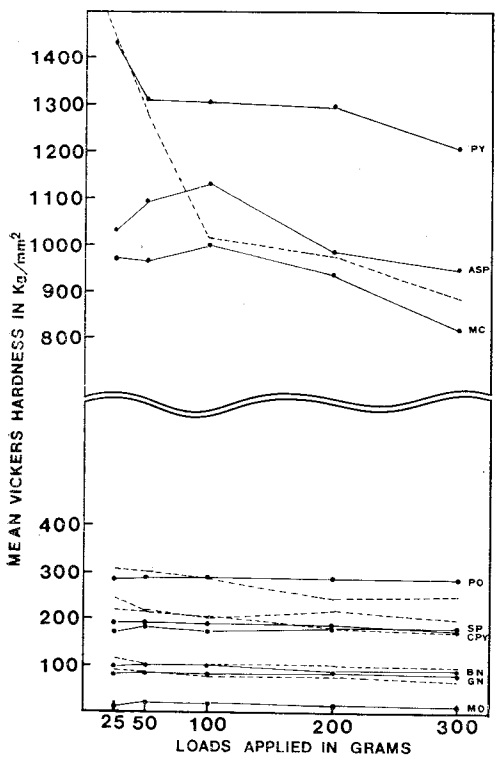

Fig. 12 Variation of average Vickers hardness number for each sulfide studied (solid line: present study; dashed line: data from Nakhla, 1956).

Chalcopyrite presents decreasing hardness number in the sequence hydrothermal vein–> skarn stage (Fig. 10). Fig. 11 demonstrates the relation between the diagonal length of Vickers indentations and the various testing weights, plotted together with data by Nakhla(1956). Results for the present study are in good agreement with those of Nakhla (1956).

Fig. 12 illustrates the relation between Vickers hardness (kg/mm^2) of the studied minerals in relation to test loads, plotted together with data by Nakhla (1956). The soft minerals such as pyrrhotite, chalcopyrite, sphalerite, bornite, galena, and molybdenite represent little hardness variation with different loads, while the hard pyrite shows remarkable variation.

Indentation shapes and fracture characteristics of the sulfides: Study of the shape and fracturing characteristics of microhardness impressions, obtained with the Vickers indenter, has been found to give useful additional information in the field of mineral determination and systematic identification procedures. In addition, several of their features help to explain the actual mode of behaviour of minerals during deformation processes.

Theoretically, the shape of a perfect Vickers indentation is that of a square in a substance

Table 6 Categories of indentation shape and fracture characteristics.

Minerals Studied	Characteristics of Indentation				Characteristics of fractures
	Straight	Concave	Convex	Sigmoidal	
Galena	Com.	St.	—	Wk.	Wk. Star rad. & Wk. GPT
Bornite	Wk.	St.	—	—	St. partings: developed along (111) planes
Sphalerite	—	St.	—	Wk.	St. Star rad. & Wk. side rad.
Molybdenite	Wk.	Wk.	Wk.	Com.	Concentric Shells
Chalcopyrite	Wk.	St.	—	—	St. Star rad.
Pyrrhotite	Wk.	St.	very Wk.	Wk.	St. Star rad. & Wk side rad. Wk. GPT
Pyrite	St.	Wk.	—	—	St. Shells & Wk. Star rad.
Arsenopyrite	Com.	Com.	—	—	Wk. Star rad. & Shells
Marcasite	St.	Wk.	—	—	St. Shells & Star rad.

*Abbreviation: Wk.: Weak; St.: Strong; Com.: Common; Rad.: Radial fractures; Shells: Shell fractures; Partings: Parting fractures; GPT: glide plane traces

having perfect plasticity; in practice the majority of minerals diverge from this ideal straight-sided shape. The many different shapes that are formed consist essentially of various combinations of four distinct shapes (Young and Millman, 1964); the straight edge, the concave edge, the convex edge, and the sigmoidal edge.

Deformation of ore minerals takes place by plastic and/or elastic processes, and may or may not be accompanied by rupture of the sturcture. Rupture of the mineral structure takes place by cracking and fracturing around and adjacent to the site of indentation. The various types of fractures have been categorized as follows (Young and Millman, 1964); radial fractures, cleavage fractures, parting fractures, simple shell fractures, cleavage shell fractures, concentric shell fracture. The results are illustrated in Table 6.

Relationships between reflectance and Vickers hardness values: Gray and Millman (1962) produced a useful mineral groupings for identification of ore minerals applying reflectivity microhardness data measured on the same area. Fig. 13, the 615nm reflectivity-range plot against the mean microhardness values was in good agreement with the results outlined by Gray and Millman (1962). The reflectivities and vickers microhardness numbers measured for the sulfide

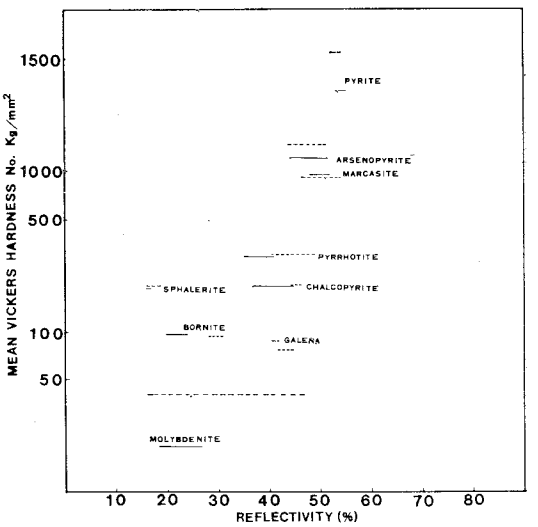

Fig. 13 Plot of mean microhardness values and 615nm reflectivity ranges (solid line: present study; dashed line; data after Gray and Millman, 1962).

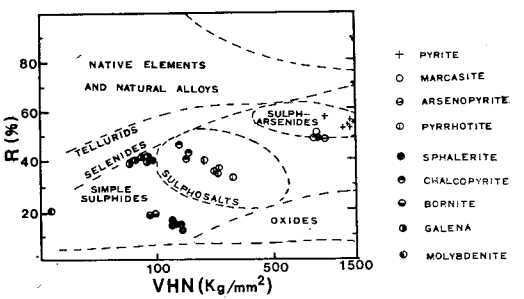

Fig. 14 Broad radicle grouping of opaque minerals on a basis of reflectivity-microhardness values, made by Gray and Millman (1962).

species are mostly plotted within the area closely corresponding to the area points made by Gray and Millman(1962) (Fig. 14).

REFERENCES

Barnes, H.L., ed. (1979) Geochemistry of hydrothermal ore deposits, 2nd ed. New York, Wiley, p. 798.

Cameron, E.N. (1963) Optical symmetry from reflectivity measurements. Am. Mineral., v. 48, p. 1070-1079.

Chi, S.J. (1984) Mineralogy and Geochemistry of Cu-Pb-Zn-Ag Hydrothermal Vein Deposit in Upper Cretaceous Volcanic Rocks of Gyeong Sang Basin. unpubl. Ph.D. Thesis, Korea Univ., p. 95.

Choi, S.G. (1983) Skarn Evolution, and Iron-Tungsten Mineralization and the Associated Polymetallic Mineralization at the Ulsan Mine, Republic of Korea, unpubl. Ph.D. Thesis, Waseda Univ., p. 270.

Craig, J.R., and Vaughan, D.J. (1981) Ore Microscopy and Ore Petrograph. John Wiley & Sons, Inc., p. 406.

Dick, L.A., and Hodgson, C.J. (1982) The MacTung W-Cu(Zn) Contact Metasomatic and Related Deposits of the Northeastern Canadian Cordillera. Econ. Geol., v. 77, p. 845-867.

Gray, I.M., and Millman, A.P. (1962) Reflection characteristics of ore minerals. Econ. Geol., v. 57, p. 325-349.

Greenwood, R. (1943) Effect of Chemical impurity on Scheelite fluorescence. Econ. Geol., v. 38, p. 56-64.

Hellingwerf,, R.H. (1984) Paragenetic zoning and genesis of Cu-Zn-Fe-Pb-As sulfide skarn ores in a proterozoic rift basin, gruvasen, western bergslagen, Sweden. Econ. Geol., v. 79, p. 696-715.

Hochella, M.F., Liou, Jr., J.G., Keskinen, M.J., and Kim, H.S. (1982) Synthesis and Stability Relations of Magnesium Idocrase. Econ. Geol., v. 77, p. 798-808.

Holland, H.D., and Malinin, S.D. (1979) The Solubility and Occurrence of non-ore minerals. In Barnes, H.L. (ed.) Geochemistry of hydrothermal ore deposits, 2nd ed., New York, Wiley, p. 789.

Hsu, L.C. (1977) Effects of Oxygen and Sulfur Fugacities on the Scheelite-Tungstenite and Powellite-Molybdenite Stability Relations. Econ. Geol., v. 72, p. 644-670.

Hsu, L.C., and Galli, P.E. (1973) Origin of the Scheelite-Powellite Series of Minerals. Econ. Geol., v. 68, p. 681-696.

Investigation Corps of the Taebaegsan Region (1962) Reports on the Geology and Mineral Resources of the Taebaegsan Region. Geological Society of Korea, p. 89.

Kim, O.J., Lee, H.Y., Lee, D.S., and Yun, S.K. (1973) The Stratigraphy and geologic structure of the great limestone series in Gangweondo, South Korea. Korean Inst. Min. Geol. J., v. 6, p. 81-114.

Kim, Y.J. (1979) Petrological Study on the Jecheon Granite Mass. Korean Inst. Min. Geol. J., v. 12, p. 115-126.

Mathieson, G.A., and Clark, A.H. (1984) The Cantung E Zone Scheelite Skarn Orebody, Tungsten, Northwest Territories: A Revised Genetic Model. Econ. Geol., v. 79, p. 883-901.

Nakhla, F.M. (1956) The hardness of metallic minerals in polished section. Econ. Geol., v. 51, p. 811-827.

Newberry, R.J., and Einaudi, M.T. (1981) Tectonic and geochemical setting of tungsten skarn mineralization in the Cordillera. Arizona Geol. Soc. Digest. v. 14, p. 99-112.

Oh, M.S., and Park, K.H. (1983) On the Genesis of Skarn-type Scheelite Deposits at the Dongmyoung mine. Korean Inst. Min. Geol. J., v. 16, p. 37-49.

Park, M.E. (1984) Mineralogic, Fluid Inclusion and Stable Isotope Studies of the Sambo Lead-Zinc-Barite Deposits. unpubl. Ph.D. Thesis, Korea Univ., p. 103.

Reedman, A.J. (1975) The age of the Gabsan Formation. Jour. Geo. Soc. Korea, v. 11, p. 139-143.

Reedman, A.J., and Um, S.H. (1975) Geology of Korea. Geological and Mineral Institute of Korea, p. 139.

Robertson, F. and Van Meter, W.J. (1951) The Kentron Microhardness Tester, A Quantitative tool in Opaque Mineral Identification. Econ. Geol., v. 46, p. 541-550.

Russell, M.C. (1975) Alteration-Mineralization Zoning, Red mountain Arizona. Econ. Geol., v. 70, p. 1437-1447.

Sato, K. (1980) Tungsten Skarn Deposit of the Fujigatani Mine, Southwest Japan. Econ. Geol., v. 75, p. 1066-1082.

Shimazaki, H. (1980) Characteristics of Skarn Deposits and Related Acid Magmatism in Japan. Econ. Geol., v. 75, p. 173-183.

Shoji, T. and Sasaki, N. (1978) Fluorescent Color and X-ray Powder Data of Synthesized Scheelite-Powellite Series to Determine its Composition. Mining Geology, v. 28, p. 397-404.

So, C.S., and Park, M.E. (1979) The Mineralogical and Geochemical Study on Korean Scheelites and its Application to the Ore Prospecting. Korean Inst. Min. Geol. J., v. 12, p. 79-93.

So, C.S., Kim, I.K., and Kim, D.H. (1980) Spectral reflectivity and microhardness of some anisortopic ore minerals from sulfide and iron deposits, Korea. Jour. Geo. Soc. Korea, v. 16, p. 16-31.

So, C.S., and Song, S.H. (1981) Physical properties of Korean ore sulfide species. Hour. Geo. Soc. Korea, v. 17, p. 1-14.

So, C.S., Lee, S.M., and Doh, S.J. (1982) Reflection-Microhardness Characteristics and Optical Symmetry of some Ore Minerals. Jour. Geo. Soc. Korea, v. 18, p. 55-66.

Stanton, R.L. (1972) Ore Petrology. McGraw-Hill Book Company, p. 713.

Uchida, E., and Liyama, T. (1982) Physicochemical Study of Skarn Formation in the Shinyama Iron-Copper Ore Deposit of the Kamaishi Mine, Northeastern Japan. Econ. Geol., v. 77, p. 809-822.

Westra, G. (1982) Alteration and Mineralization in the Ruth Porphyry. Copper Deposit near Ely, Nevada. Econ. Geol. v. 77, p. 950-970.

Young, B.B., and Millman, A.P. (1964) Microhardness and Deformation Characteristics of Ore Minerals. Trans. Inst. Min. Metall., v. 73, p. 437-466.

東明重石鑛山産 硫化鑛物의 鑛物學的 硏究

李甸九・蘇七燮・金世鉉・尹聖澤・金炆榮

요약：스카른형 東明灰重石鑛床은 朝鮮系 大石灰岩統에 대비되는 三台山層과 이를 관입한 쥬라기 花崗閃綠岩과의 접촉대에 발달한 接觸交代鑛床이다. 鑛化作用은 스카른시기, 열수시기, 후기열수시기의 3회에 걸쳐 진행되었으며, 접촉부로부터 규회석, 투휘석, 투회석—석류석, 석류석, 베스비아나이트 스카른帶가 불규칙한 帶狀分布한다. 灰重石은 규회석스카른을 제외한 모든 스카른帶와 열수시기초기 石英脈에서 산출되며, 특히 磁硫鐵石, 方鉛石, 베스비아나이트와 밀접하게 共生한다. 즉 磁硫鐵石이 침전되면서 유리되 나온 水素이온은 모암인 石灰岩과 反應, 분리된 Ca이온의 活性度가 증가되며 灰重石이 침전된 것으로 사료된다.

한편 東明鑛山産 主및副成分 硫化鑛物을 대상으로한 物性실험 연구를 통하여, 鑛化時期 및 鑛物의 內部反射현상에 따른 反射度・微硬度의 상관성을 검토하고 光學的 對稱性을 연구하여 황동석과 백철석은 2軸性(−), 반동석은 2軸性(+)임을 밝혔으며 유비철석은 2軸性이나 對稱性을 결정할 수 없었다. 微硬度실험에서는 硬度가 낮은 광물일수록 하중에 따른 微硬度값의 변화경향이 적으며, 실험된 광물은 모두 특징적인 indentation을 보여 광물감정에 이용될 수 있을 것으로 고려된다.